Int J Adv Manuf Technol (2015) 78:573–581
DOI 10.1007/s00170-014-6678-6

ORIGINAL ARTICLE

Groove sidewall penetration modeling for rotating arc narrow gap MAG welding

Wenhang Li · Kai Gao · Jing Wu · Jiayou Wang · Yunhong Ji

Received: 13 May 2014 / Accepted: 1 December 2014 / Published online: 10 December 2014
© Springer-Verlag London 2014

Abstract It is important to predict the groove sidewall penetration for narrow gap MAG welding quality control. In this paper, we present a hybrid model to describe the groove sidewall penetration dynamics. First, sensing system was set up to obtain and fuse the signal from arc sensor, visual sensor, and sidewall penetration sensor. Next, the center position of the rotating arc was varied to generate the experimental data. Due to the fact that sidewall penetration on the left side varies greater than that on the right side, a support vector machine (SVM)-based dynamic model was built to predict the penetration on the left side and a cubic polynomial regression model for the right side. The model developed in this paper can be applied to the further penetration control.

Keywords Rotating arc · Narrow gap MAG welding · Penetration modeling · Support vector machine

1 Introduction

As a highly efficient welding method, rotating arc narrow gap MAG welding (RA-NGMW) [1–3] requires enough penetration on both sides of the groove wall. Building a dynamic prediction model for sidewall penetration is significant for its quality control [4].

There are many research for penetration control whether in GTAW or GMAW in the field of sensing, modeling, and control method [5–10]. For RA-NGMW, its sidewall penetration is hard to be observed or modeled; therefore, some research focus on the forming of weld seam under different constant parameters, which is useful for a static model rather than a dynamic model.

Theoretically, the sidewall penetration is mainly decided by the endothermic and radiating. Here, the radiating is supposed to be same, and the endothermic is mainly affected by the thermal arc and the absorption rate. It is well known that the thermal arc is decided by welding current when the arc length is relatively long. For absorption rate, it was mainly decided by the shortest distance of "sidewall arc center" and the angle of droplet transfer, which will affect the heat transition to the sidewall whether by liquid metal convection or plasma stream. Usually, the angle of droplet transfer is constant in welding [11]. Therefore, welding current and distance of sidewall arc center were selected as the input and penetration as the output.

Considering the complexity of welding process, a support vector machine (SVM) [12, 13] modeling method was used to build the dynamic model.

Another challenge for building dynamic model is that the penetration information is obtained off-line while other information is obtained on-line. It is necessary to fuse the penetration information with the rest using equipment and method as designed in this paper.

In this paper, we built a dynamic model for sidewall penetration of RA-NGMW. The remainder of the paper is organized as follows. In Sect. 2, the RA-NGMW welding and sensing systems were introduced. In Sect. 3, experiments were designed, and data were obtained. In Sects. 4 and 5, an SVM model for left sidewall penetration and a regression model for right sidewall penetration were built, respectively. Sect. 6 concludes this paper.

W. Li (✉) · K. Gao · J. Wang · Y. Ji
School of Materials Science and Engineering, Jiangsu University of Science and Technology, Zhenjiang 212003, Jiangsu Province, China
e-mail: lwh_abc@qq.com

W. Li
Jiangsu Modern Shipbuilding Technology Co., Ltd., Zhenjiang 212003, China

J. Wu
Department of Mechanical Engineering, Aerospace and Biomedical Engineering, The University of Tennessee, Knoxville, TN 37996-2210, USA

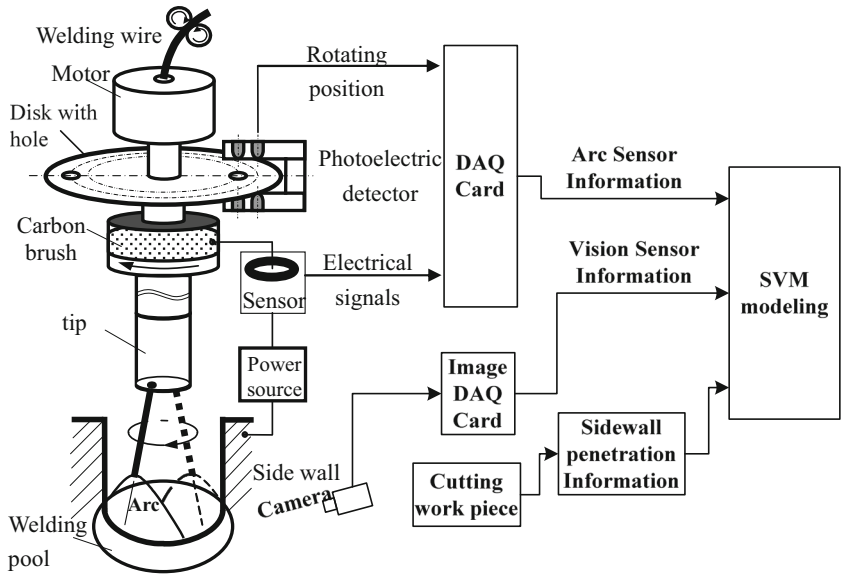

Fig. 1 Structure of welding torch and sensing information for modeling

Table 1 Welding parameters of narrow gap MAG welding

Parameter	Value
Torch height *H*, mm	20
Wire diameter, mm	1.2
Workpiece	Q235
Power source external characteristic	Constant-voltage
Welding current *I*, A	300 (setting value)
Welding voltage *U*, V	31
Welding speed *v*, mm/min	230
Shield gas flow meter *q*, L/min	30
Rotating frequency *f*, Hz	50

2 RA-NGMW welding and sensing systems

The RA-NGMW and its sensing system are shown in Fig. 1. For the rotating arc torch, the tip had a bias hole, which made the end of wire deviate the tip axis and the arc rotate during welding. The detail principle of welding torch can be found in Wang's work [1]. The welding parameters are shown in Table 1.

As to the sensing part, Hall current sensor was used to obtain welding current. Second, a photoelectric switch and a hole on a disk (fixing on the rotating part of torch) were combined to detect the arc position when it was in the front of welding pool. Third, a CCD camera was placed in front of welding pool to obtain the welding image [14], and the shortest distance of sidewall arc center was obtained by image processing. The detail of sensing information acquisition and deal were introduced as following.

2.1 Arc sensing information

Here, welding current was obtained by current hall sensor. Then, the sensing signal was input to the NI PCI-6251 DAQ card and processed by PC. Although the welding current was set as constant value in the power source, the welding current varied according to the variation of arc length. It was obvious that we should select the current whose position was near the groove sidewall. Here, the left and right 1/4 rotating circle parts were selected as the signal extraction area as shown in

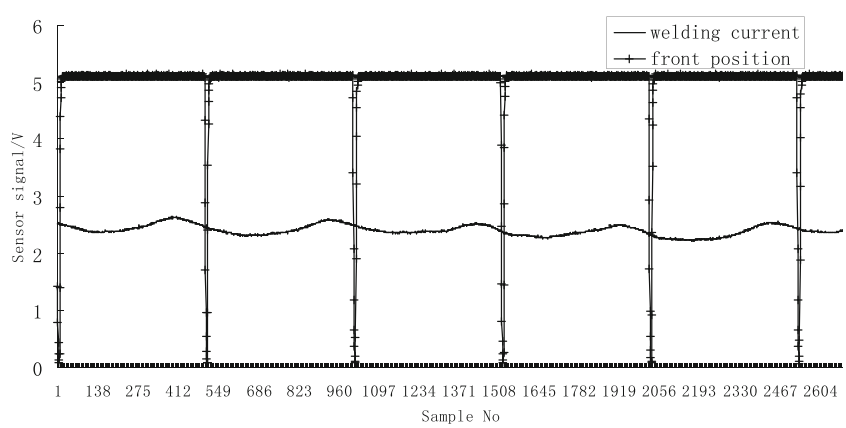

Fig. 2 Obtained current signal and front position signal

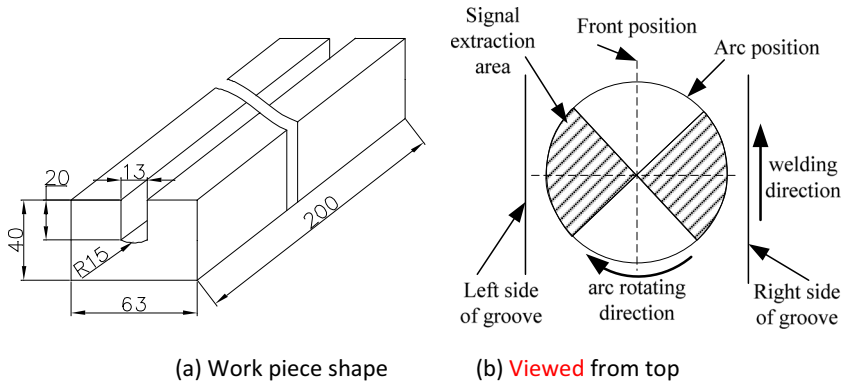

Fig. 3 Current signals extracting in an arc rotation period. **a** Workpiece shape. **b** Viewed from top

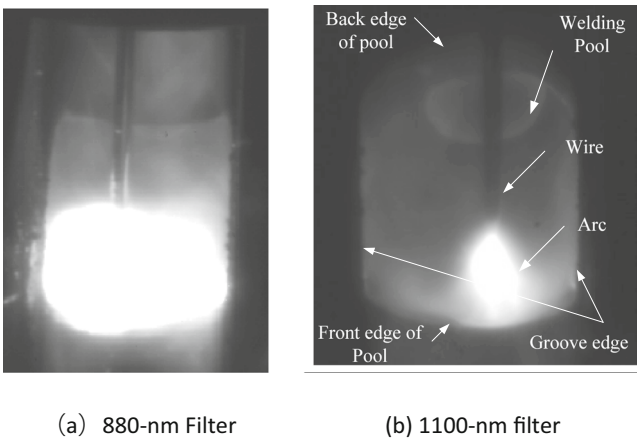

Fig. 4 Infrared region welding image of rotating arc MAG welding. **a** 880-nm filter. **b** 1100-nm filter

Fig. 3. In addition, the arc's front position signal was used to identify this area. The obtained current signal and front position signal are shown in Fig. 2. The mean value was used to represent the welding current near the sidewall (Fig. 3).

2.2 Vision sensing information

To get the shortest distance of sidewall arc center, we need to get and process the welding image. Here, passive vision was adopted, and the infrared image was taken to weaken the arc light and improve the metal radiation relatively. Figure 4 shows two welding images with different filter. For Fig. 4a, the welding wire and weld pool were clearer, but the arc area was too large to determine the arc position. For Fig. 4b, the end position of wire is visible in the image, but it is sensitive to the welding conditions; on the other hand, the arc light area is small and robust to detect. Therefore, we use the arc light area to determine the arc position. In detail, the camera model was MV1-D1312I-C031-160-CL whose exposure time was 5 ms and aperture was 7. The optical filter's center wavelength was 1100 nm, and its width was 20 nm, and ND filter's pass rate was 10 %.

Typical gray histogram of welding image is shown in Fig. 5, where the first peak on the left (part B) represents the groove and the dark area above the arc in Fig. 4b; the second peak on the left (part C) represents the brighter areas in the groove in Fig. 4b; and the peak on the right (part D) represents arc bright area in the groove in Fig. 4b. Therefore, the arc and the groove area can be segmented by threshold. More specifically, the gray value of the valley between the first and second peak was set as the first threshold to detect sidewall and the gray value of the right peak as the second threshold to detect the arc center position.

Since the narrow groove is approximately vertical, only the detection of horizontal edge is necessary in the edge detection of groove sidewall. According to features of the image in Fig. 4, the sidewall edge detection area could be divided into

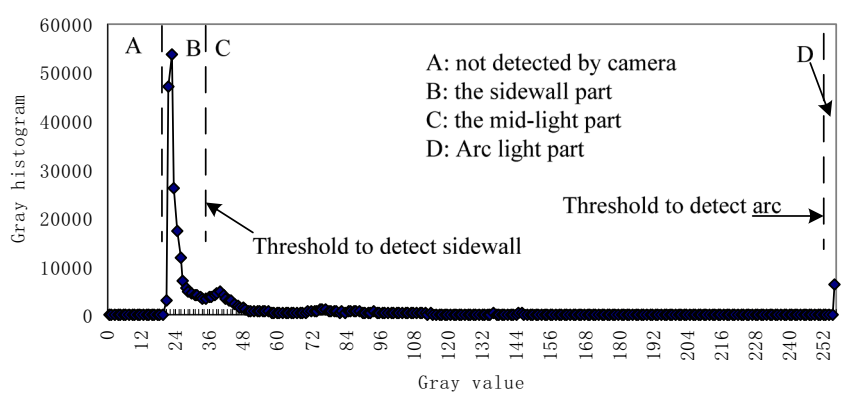

Fig. 5 The gray histogram of welding image

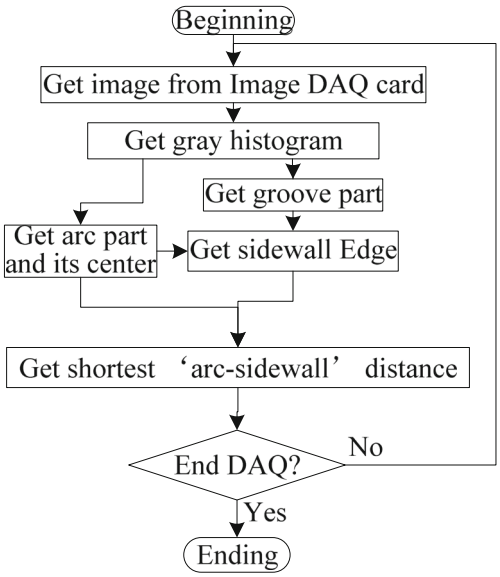

Fig. 6 Deviation detection algorithm of vision sensing

three areas: (1) the upper area of the sidewall, where the edge was hard to distinguish because the arc light there was relatively weak; (2) the middle area of sidewall, where its horizontal position near that of the arc and the edge was easy to distinguish since the arc light was enough; (3) the lower area of the sidewall, where the bright part in groove became narrow and could not accurately represent the groove sidewall edge. Therefore, the arc center was determined as first, and then, the sidewall edge was detected near the arc's vertical position. Using a simple first-order difference, the sidewall edge can be easily calculated (Fig. 6).

In order to improve the efficiency of the algorithm, the edge detection could be implemented only on several lines in the image as shown in Fig. 7, whose vertical position was near that of arc center.

After extractions of the groove sidewall's left and right edge and the arc's horizontal position, the groove center was extracted by computing the mean values of groove sidewall's left and right position. The arc's rotating center was extracted by calculating the mean value of arcs' horizontal positions in two consequent images. The difference between the arcs' rotating center and the groove center was the weld deviation. Figure 6 shows the flow chart of vision-based deviation extraction. Figure 7 shows two captured images in an arc rotation period with its image processing result.

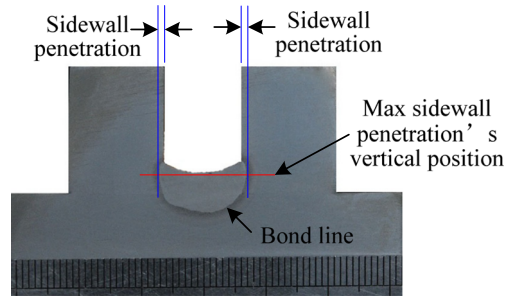

Fig. 8 Section image by the plane perpendicular to the direction of welding. **a** Overall view. **b** Partial enlarged view

Finally, to fuse the signal from different sensors, it was necessary to simultaneously acquire and analyze arc sensing and vision sensing information in each rotation period. Because the data acquisitions of arc sensing and vision sensing were triggered by the arc position signal, the synchronization was easy to realize.

2.3 Sidewall penetration information

In the conventional practice, it is necessary to cut the workpiece with the plane perpendicular to the direction of welding so as to obtain the fusion line and detect the welding penetration, as shown in Fig. 8. This is infeasible when the penetration varies significantly. Therefore, we made the cutting plane parallel to the bottom of the workpiece, and we need to know the proper plane position. Figure 8 shows that the max sidewall penetration's vertical position was near the bottom of weld seam, and the according section image is shown in Fig. 9.

Another problem was that we need to make the penetration information synchronous with the DAQ information. So, we need to get the position on workpiece when the DAQ started

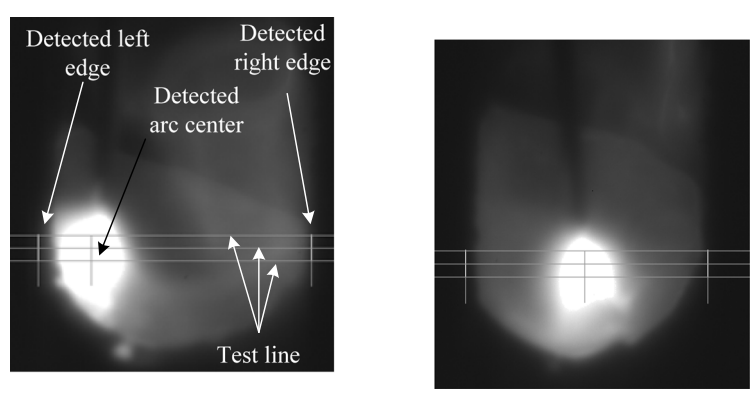

(a) Image when arc on one side of pool (b) Image when arc on the another side of pool

Fig. 7 Two continuous captured images in a rotation period. **a** Image when arc on one side of pool. **b** Image when arc on the another side of pool

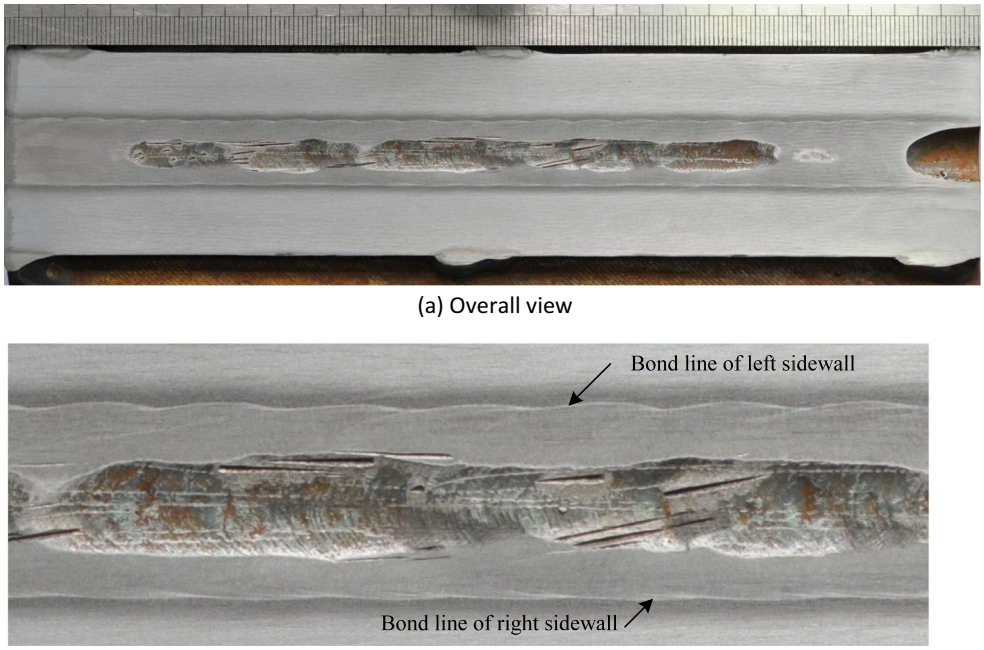

(a) Overall view

(b) Partial enlarged view

Fig. 9 Section image by the plane parallel to bottom of workpiece

and ended. Thus, special equipment was designed as shown in Fig. 10.

The equipment was made up of scriber fixed on the rod of mini cylinder. The scriber was pushed down to the dashboard by air pressure when the data acquisition started until the data acquisition end; so, there was a nick on the dashboard.

The arc rotation center and the scriber ends have the same projection on the welding direction; so, the start and end position of data acquisition can be marked on the workpiece.

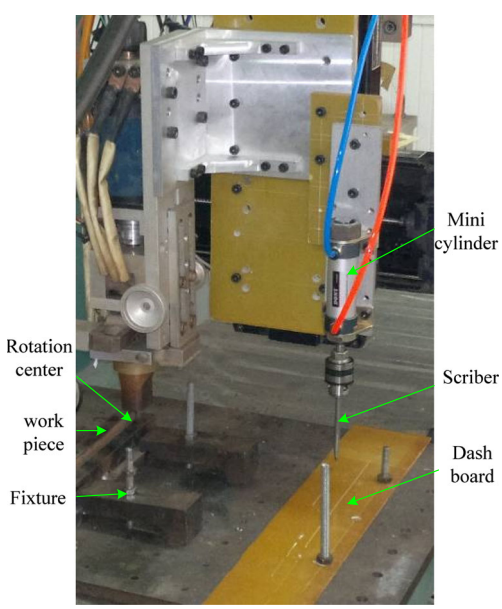

Fig. 10 Equipment to mark the start and end of data acquisition

A complete curve of the bond line was needed to obtain the penetration position. Due to low contrast in the heat-affected zone, results from automatic edge detection algorithm were not satisfactory. Therefore, we used an interactive method to obtain input points by mouse hit. The manually obtained points were then interpolated by cubic spline curve fitting to get the penetration in any time. Figure 11 shows the bond line's fitting result by spline curve.

3 Experiments

For narrow gap welding, welding current was set at constant value so as to ensure good welding formation, but it may vary when the arc length changes in arc rotation, as shown in Fig. 2.

To build a dynamic model of side wall penetration, the position of arc rotating axis was waved as shown in Fig. 12 and Table 2.

The welding current, arc sidewall shortest distance, and sidewall penetration were obtained by the methods shown in Sect. 2. Figure 9 shows one image of bond line. From the result in Fig. 9b, the left sidewall penetration varied more than that of right sidewall. The cause might be that the welding pool was declining, and the clockwise rotating arc's power was easy to remove the molten iron in left side but hard to remove that in right side. Therefore, the arc power was easy to affect the left side and hard to affect the right side, and we needed to build two separated model for left and right sidewall penetration, respectively.

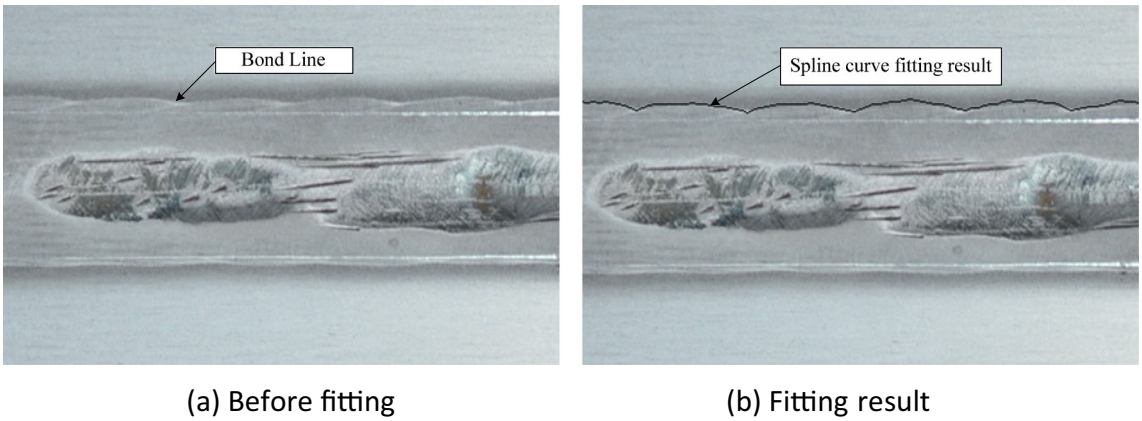

Fig. 11 Spline curve fitting for bond line

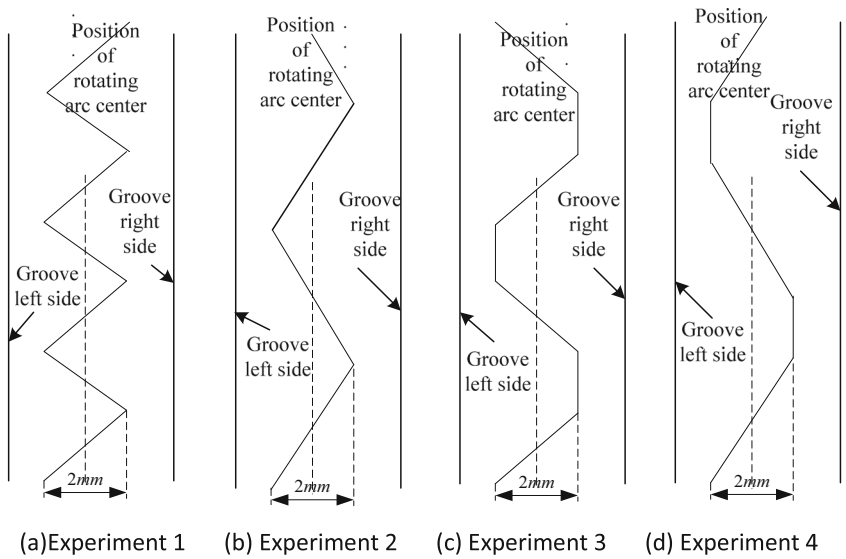

Fig. 12 Position of rotating arc center. **a** Experiment 1. **b** Experiment 2. **c** Experiment 3. **d** Experiment 4

4 Left sidewall penetration model

Since the left sidewall penetration varied more, it was necessary to build a dynamic model. Considering the high complexity of welding process, an SVM method was used to build the model.

4.1 SVM-based modeling method

Figure 13 shows the procedure of SVM modeling method. The SVM-based modeling method began with acquiring

Table 2 Weaving parameter planning

Experiment no.	Residence time at side wall/s	Wave time/s	Swing amplitude/mm
1	0	1	1
2	0	2	1
3	0.5	1	1
4	0.5	2	1

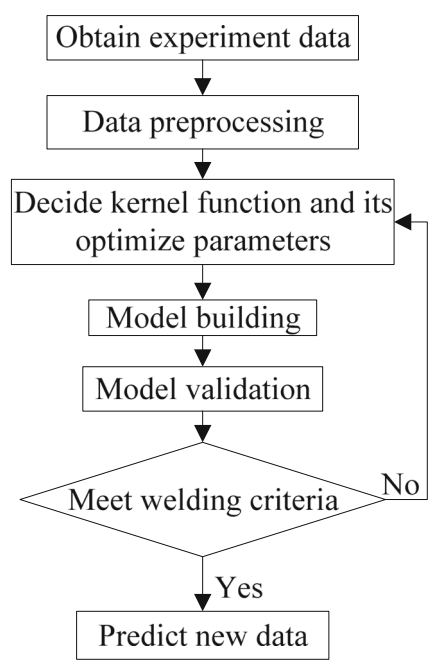

Fig. 13 Procedure of the SVM modeling method

Table 3 Partial SVM data

Sample no.	Input variable I/A					Input variable W/mm					Output P/mm
	I^{t-9}	I^{t-8}	…	I^{t-1}	I^{t}	D^{t-9}	D^{t-8}	…	D^{t-1}	D^{t}	
600	301.4	298.7	…	292.7	302.0	3.66	4.00	…	5.13	4.46	1.177
601	298.7	297.5		302.0	301.8	4.00	4.30		4.46	4.07	1.063
602	297.5	300.7		302.8	308.0	4.30	4.98		4.07	3.61	0.937
603	300.7	298.1		308.0	304.2	4.98	5.38		3.61	3.27	0.833
604	298.1	300.6		304.2	304.1	5.38	5.42		3.27	3.16	1.037
605	300.6	296.1		304.1	302.6	5.42	5.32		3.16	3.05	1.277

Table 4 Correlation analysis

Input variable	Correlation coefficient	Input variable	Correlation coefficient
I^{t-9}	0.1188	W^{t-9}	0.1369
I^{t-8}	0.1325	W^{t-8}	0.1523
I^{t-7}	0.1445	W^{t-7}	0.1549
I^{t-6}	0.1548	W^{t-6}	0.1425
I^{t-5}	0.1739	W^{t-5}	0.1197
I^{t-4}	0.1907	W^{t-4}	0.0888
I^{t-3}	0.2092	W^{t-3}	0.0465
I^{t-2}	0.2188	W^{t-2}	−0.0007
I^{t-1}	0.2187	W^{t-1}	−0.0504
I^{t}	0.2111	W^{t}	−0.0986

experiment data. Second, the obtained data was preprocessed, where the denoising method was used to improve the data quality and the normalization was used to decrease the influence of large value data. Third, the experimental data were used to build SVM model by deciding kernel function and optimizing its parameters. When the SVM model met the criteria of the welding application, it was used to predict the sampling data on-line.

4.2 Input variable selection

The welding current I, arc left sidewall shortest distance D, and penetration P were obtained as discussed in Sect. 2. Part data are shown in Table 3. Since there was delay between welding current and sidewall penetration, we extended the model with I form I^{t} to I^{t-9} and D from D^{t} to D^{t-9}. Table 4 shows the correlation coefficient between input variables and output variable. It showed that the current I's correlation increased until I^{t-5} and distance D's correlation increased until I^{t-5}.

According to the results in Fig. 14, four groups of input with different delay were experimented, as shown in Table 5. By comparing the mean squared error (MSE) and mean absolute error (MAE) of each group from SVM prediction, we select group 3 as the final model due to its best performance, and the input variables were "I^{t-4}, I^{t-3}, I^{t-2}, W^{t-4}, W^{t-3}, W^{t-2}."

4.3 SVM parameter optimization

There are four types of frequently used kernel functions for mapping data into high dimensional space, namely, linear, polynomial, radial basis function (RBF), and sigmoid kernels. RBF kernel was used in this paper due to its wide application [15, 16]. For RBF kernel, width gamma (γ) and penalty parameters (C) are two of the most important parameters. C, a regularization parameter, controls the tradeoff between maximizing the margin and minimizing the training error. Too small value of C may not give enough penalties on the outliers, while too large value of C leads to over fitting. Usually, C should be set large enough to have a stable training process. The parameter γ affects the number of support vector, which has a close relation with the training time. Too many

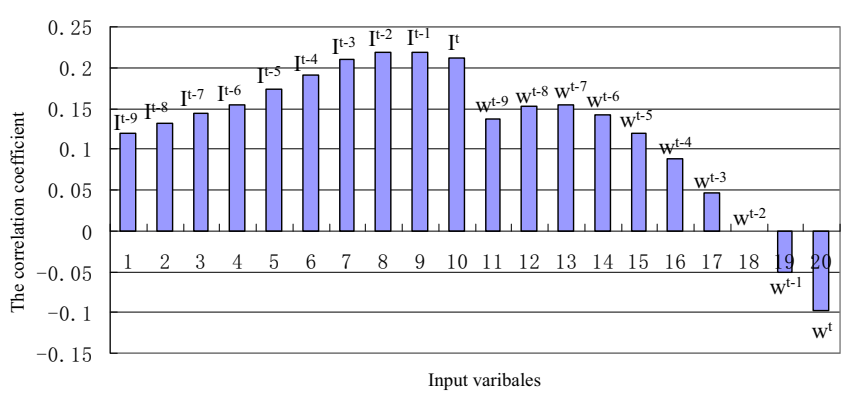

Fig. 14 The bar graph of correlation analysis

Table 5 SVM parameters and prediction result for different input variable

Model No	Input factor group	C	γ	MSE	MAE
1	I^t, w^t	0.1768	22.6274	0.1365	0.3050
2	$I^{t-2}, I^{t-1}, I^t, w^{t-2}, w^{t-1}, w^t$	1.4142	4	0.1205	0.2852
3	$I^{t-4}, I^{t-3}, I^{t-2}, w^{t-4}, w^{t-3}, w^{t-2}$	0.3536	8	0.1154	0.2782
4	$I^{t-6}, I^{t-5}, I^{t-4}, w^{t-6}, w^{t-5}, w^{t-4}$	0.4142	4	0.1186	0.2796

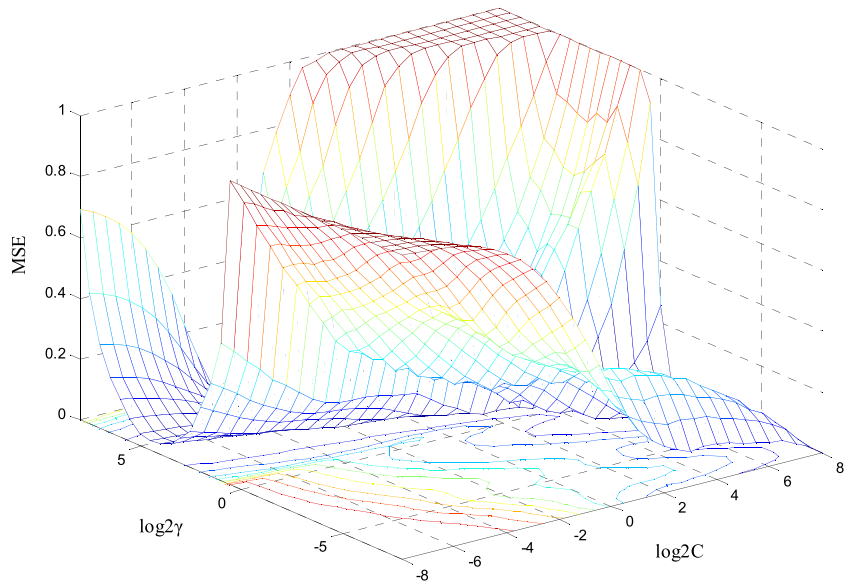

Fig. 15 Prediction results of different parameters

support vectors can produce over fitting and extend training time. Parameter γ also controls the amplitude of the Gaussian function and, therefore, affects the generalization ability of SVM [17]. In this study, the parameters of RBF were determined by a grid search method based on cross-validation. The main idea is to test the different parameters and select the one with the highest cross-validation accuracy. The method was conducted in two steps. In the first step, a coarser grid was applied with an exponentially growing sequence of C, γ with $C=2^{-8}, 2^{-7.2}, 2^{-6.4}, \ldots, 2^{6.4}, 2^{7.2}, 2^{8}$ and $\gamma=2^{-8}, 2^{-7.2}, 2^{-6.4}, \ldots, 2^{6.4}, 2^{7.2}, 2^{8}$. In the second step, after identifying the optimal region on the grid, the finer grid search was executed. The results were used to perform the final training process. Here, three-fold cross-validation method was used to find optimal parameters. The 3D image of C, γ, and forecast accuracy is shown in Fig. 15, where the optimal parameters were C=0.3536, γ=8. Then, the SVM model was built by using the optimal parameters.

Table 6 Experiment sensor data for right side penetration

Experiment no.	Current I/A	Arc side width/mm	Penetration P/mm
1	297.978	6.210	0.53
2	298.524	4.727	0.87
3	300.233	5.622	0.65
4	304.293	3.354	1.19
5	298.558	3.904	1.04
6	322.383	2.492	2.0

4.4 Model validation

Ten-fold cross-validation was used to validate the proposed model, with results shown in Table 5, where MSE was mean square error and MAE was mean abstract error.

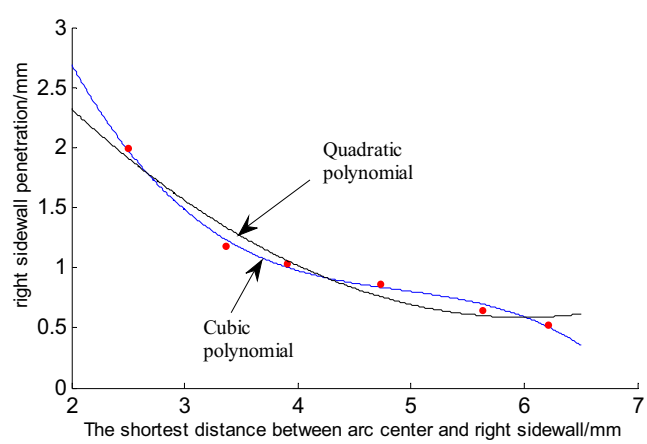

Fig. 16 The result drawing of curve fitting

5 Right sidewall penetration model

As shown in Fig. 10, the right side penetration varied less than that of left side. Obviously, it was not necessary to build a dynamic model, and a static model was built. The right sidewall penetration was obtained by the similar setting as the left one, but the weld deviation was set differently. The obtained data are shown in Table 6. Although we set the welding current as constant value, it will vary for the variation of arc length. However, the variation of welding current was less than that of arc length. So, we used the arc side width to make a regression prediction for the penetration as Fig. 16. It showed the cubic polynomial performed better than that of quadratic. The following was the cubic polynomial regress model.

$$w = -0.0617d^3 + 0.9074d^2 - 4.5744d + 8.7061$$

The equation was a regression model for the right side penetration with the welding current equal to 300 A.

6 Conclusion

Some conclusions were drawn as following:

1. Synchronous acquisition system was set up to realize the synchronization of the arc sensor, image sensor, and sidewall penetration.
2. An interesting phenomena was found that the left sidewall penetration varied more than that of the right side.
3. An SVM-based dynamic model was built for the prediction of the left sidewall penetration, and a cubic polynomial regression model was built for the prediction of the right sidewall penetration.

Acknowledgments The authors would like to thank the financial support from the National Natural Science Foundation of China (No 51005107, 51475218), Natural Science Foundation of Jiangsu Province (No. BK2011509), Specialized Research Fund for the Doctoral Program of Higher Education (20133220110001), the Qing Lan Project of Jiangsu province for outstanding young teachers and technology innovation team.

References

1. Wang JY, Ren YS, Yang F, Guo HB (2007) Novel rotation arc system for narrow gap MAG welding. Sci Technol Weld Join 12(6):505–507
2. Min D, Xin-hua T, Feng-gui L, Shun Y (2011) Welding of quenched and tempered steels with high-spin arc narrow gap MAG system. Int J Adv Manuf Technol 55(5–8):527–533
3. Yang CL, Guo N, Lin SB, Fan CL, Zhang YQ (2009) Application of rotating arc system to horizontal narrow gap welding. Sci Technol Weld Join 14(2):172–177
4. Kim GH, Na SJ (2001) A study of an arc sensor model for gas metal arc welding with rotating arc part 1: dynamic simulation of wire melting. Proc Inst Mech Eng B J Eng Manuf 215(9):1271–1279
5. Bentley AE, Marburger SJ (1992) Arc welding penetration control using quantitative feedback theory. Weld J 71:397–405
6. Nagesh DS, Datta GL (2002) Prediction of weld bead geometry and penetration in shielded metal-arc welding using artificial neural networks. J Mater Process Technol 123(2):303–312
7. Chen SB, Zhao DB, Wu L, Lou YJ (2000) Intelligent methodology for sensing, modeling and control of pulsed GTAW: part 2–Butt joint welding. Weld J (USA) 79(6):164–174
8. Fan C, Lv F, Chen S (2009) Visual sensing and penetration control in aluminum alloy pulsed GTA welding. Int J Adv Manuf Technol 42(1–2):126–137
9. Kim I, Basu A, Siores E (1996) Mathematical models for control of weld bead penetration in the GMAW process. Int J Adv Manuf Technol 12(6):393–401
10. Lv N, Zhong J, Chen H, Lin T, Chen S (2014) Real-time control of welding penetration during robotic GTAW dynamical process by audio sensing of arc length. Int J Adv Manuf Technol 74:235–249
11. Guo N, Lin SB, Zhang L, Yang CL (2009) Metal transfer characteristics of rotating arc narrow gap horizontal GMAW. Sci Technol Weld Join 14(8):760–764
12. Cortes C, Vapnik V (1995) Support vector machine. Mach Learn 20(3):273–297
13. Lela B, Bajić D, Jozić S (2009) Regression analysis, support vector machines, and Bayesian neural network approaches to modeling surface roughness in face milling. Int J Adv Manuf Technol 42(11–12):1082–1088
14. Ye Z, Fang G, Chen S, Zou JJ (2013) Passive vision based seam tracking system for pulse-MAG welding. Int J Adv Manuf Technol 67(9–12):1987–1996
15. Huang X, Gu W, Shi F, Chen S (2009) An adaptive inverse control method based on SVM-Fuzzy rules acquisition system for pulsed GTAW process. Int J Adv Manuf Technol 44(7–8):686–694
16. Li W, Gao K, Wu J, Hu T, Wang J (2014) SVM-based information fusion for weld deviation extraction and weld groove state identification in rotating arc narrow gap MAG welding. Int J Adv Manuf Technol 74(9–12):1355–1364
17. Zhao C, Zhang H, Zhang X, Zhang R, Luan F, Liu M, Hu Z, Fan B (2006) Prediction of milk/plasma drug concentration (M/P) ratio using support vector machine (SVM) method. Pharm Res 23(1): 41–48